



ARCHIVES  
of  
FOUNDRY ENGINEERING

DOI: 10.1515/afe-2015-0090

Published quarterly as the organ of the Foundry Commission of the Polish Academy of Sciences



ISSN (2299-2944)

Volume 15

Issue 4/2015

115 – 123

# The Effect of Shell Thickness, Insulation and Casting Temperature on Defects Formation During Investment Casting of Ni-base Turbine Blades

M. Raza<sup>a, b\*</sup>, M. Irwin<sup>b</sup>, B. Fagerström<sup>a</sup><sup>a</sup> School of Innovation, Design and Engineering, Mälardalen University, Smedjegatan 37, 632 20 Eskilstuna, Sweden<sup>b</sup> TPC Componest AB, Brånstaleden 2, 734 92 Hallstahammar, Sweden

\*Corresponding author. E-mail address: mohsin.raza@mdh.se

Received 22.05.2015; accepted in revised form 15.07.2015

## Abstract

Turbine blades have complex geometries with free form surface. Blades have different thickness at the trailing and leading edges as well as sharp bends at the chord-tip shroud junction and sharp fins at the tip shroud. In investment casting of blades, shrinkage at the tip-shroud and cord junction is a common casting problem. Because of high temperature applications, grain structure is also critical in these castings in order to avoid creep. The aim of this work is to evaluate the effect of different process parameters, such as, shell thickness, insulation and casting temperature on shrinkage porosity and grain size. The test geometry used in this study was a thin-walled air-foil structure which is representative of a typical hot-gas-path rotating turbine component. It was observed that, in thin sections, increased shell thickness helps to increase the feeding distance and thus avoid interdendritic shrinkage. It was also observed that grain size is not significantly affected by shell thickness in thin sections. Slower cooling rate due to the added insulation and steeper thermal gradient at metal mold interface induced by the thicker shell not only helps to avoid shrinkage porosity but also increases fill-ability in thinner sections.

**Keywords:** Investment casting, Casting defects, Shrinkage porosity, Grain structure, Turbine blades, Niyama criterion

## 1. Introduction

Since most nickel base super alloys have a relatively large solidification interval, an extended mushy zone is formed during solidification and melt flow is restricted between dendrites resulting in interdendritic porosity. In air-foil geometries such as turbine blades, interdendritic shrinkage porosity appears in the areas where solidification fronts meet at sharp intersections or along the centreline of the blade. Shrinkage porosity forms deep in the mushy zone in alloys with a large solidification interval.

These alloys solidify in a mushy form [1]. In the melt, crystals at various stages of growth are dispersed forming a pasty mode. At the initial stage of solidification any contraction due to the difference in density of the solidifying metal and liquid melt is compensated by mass movement of the melt, however, liquid feed becomes more difficult when a continuous mush is formed [2]. Melt feed continues to pass through narrow channels in solid mush but eventually is hindered due to the pressure drop leaving isolated pockets which cannot be compensated by liquid feed. Figure 1(a) shows the typical porosity in such a turbine blade.

Porosity due to these isolated pockets is induced primarily by difficulty in providing liquid flow required during final solidification of the solid phase which is denser than the interdendritic liquid [3]. Increasing casting temperature helps to keep the narrow channels open for longer time which helps to feed isolated pockets deep in the mush, however, increased casting temperature causes other problems, for example large grain size. Figure 1 (b) shows large grain formation at the root of blade which is adjacent to in-gate. Slower cooling as compared to the thin sections of the blade and extra heat mass at root causes large grain formation. Increasing the pressure head of metal in investment casting is also not usually practical because metallostatic pressure is often negligible as compared to the bubble pressure.



Fig. 1. Common defects in casting of turbine blades

Metallostatic pressure induced by pressure head can be calculated

$$p_m = \rho gh \quad (1)$$

where as bubble pressure can be calculated by

$$p_p - p = \frac{2\sigma}{r_p} \quad (2)$$

Since the bubble radius is usually on the order of micrometer in size and surface tension  $\sigma$  is fairly large value, usually the bubble pressure  $P_p$  is more than the metallostatic pressure.

$$p_p \geq p + \frac{2\sigma}{r_p} \quad (3)$$

which suggest that increasing pressure head in investment casting does not help significantly to avoid shrinkage and gas porosity. Darcy's law relates the velocity to pressure drop. According to Darcy's law in 1-D system

$$g_l v_l = \frac{K dp}{\mu dx} \quad (4)$$

where  $g_l$  is the liquid fraction,  $v_l$  is the liquid velocity in the mushy zone (i.e. shrinkage velocity),  $\mu_l$  is the liquid dynamic viscosity,  $p$  is the melt pressure and  $x$  is the spacial coordinate.  $K$  is permeability in the mesh zone. By integrating Darcy's law in equation 7 and substituting relation for shrinkage velocity

$$v_l = \beta R, \text{ thermal gradient } G = \frac{dT}{dx} \text{ and the isotherm}$$

$$R = \frac{T'}{G},$$

$$\begin{aligned} \Delta p &= - \int_{x_l}^{x_s} \frac{\mu}{K} g_l v_l dx = \frac{\mu \beta R}{G} \int_{T_s}^{T_l} \frac{g_l}{K} dT = c_1 \cdot \frac{R}{G} \\ &= c_1 \cdot \frac{T'}{G^2} > \Delta p_{crit} \end{aligned} \quad (5)$$

Where  $G$  is thermal gradient,  $T'$  is the cooling rate,  $\beta$  is solidification shrinkage defined as  $[\frac{\rho_s}{\rho_l} - 1]$  and  $c_1$  is integration constant. Pores forms when pressure drop exceeds critical pressure drop [4].

According to Niyama Criterion, Pores forms when

$$N_y = \frac{G}{\sqrt{T'}} < \sqrt{\frac{c_1}{\Delta p_{crit}}} \quad (6)$$

where  $N_y$  is known as the Niyama constant.

Larger freezing range causes the integral and hence the constant, to be larger, hence the pressure drop will be larger and porosity form more easily in large freezing range alloys (feeding distance would be shorter). In a simple relation, porosity forms when

$$\frac{G}{\sqrt{T'}} < const. \quad (7)$$

A large temperature gradient,  $G$ , prevents porosity because

1. The mushy zone is shorter (shorter distance to feed)
2. For the same cooling rate, the isotherm speed,  $R = \frac{T'}{G}$  is

smaller i.e. a smaller  $R$  results in a lower melt velocity,  $v_l = \beta R$  which consequently results in a lower pressure drop according to Darcy's Law.

Similarly a lower cooling rate prevents porosity because of its effect on the isotherm [5]. Feeding length can be calculated using Darcy's law however because of complexity of moving

solidification fronts, simple metallurgical calculations do not predict the length of the effective feeding distance. Existing principles for design of feeders to avoid shrinkage, for example Chovorinov's rule for feeder design, is too complex to apply in complex geometries such as turbine blades. To avoid interdendritic shrinkage it is important to minimize the mushy zone. The width of the mushy zone depends on the temperature gradient and non equilibrium freezing range of the Alloy [5].

The main focus of this study has been to evaluate the foundry parameters that can help to create conditions that are required to increase melt flow through the mush in order to avoid shrinkage porosity in complex geometries. The foundry parameters evaluated in this study were shell thickness, insulation and casting temperature. Test geometries were cast at different casting temperatures with varying shell thickness and insulation patterns to find their effect on shrinkage porosity, grain structure and fillability in thin sections. The work explains how to shell thickness and well designed insulation can help to achieve the steeper thermal gradient at metal/mould interface and slower cooling rate which is required to keep mushy zone narrow in order to facilitate feeding through the mush. The work also explains how fillability and grain structure is affected by increased shell thickness.

## 2. Experimental work

In this experimental work a typical turbine blade geometry for an industrial gas turbine was selected, with chord length of 89 mm, leading edge thickness 0.56 mm and trailing edge thickness 1.05 mm. The cluster was designed to optimize fluid flow in the cavity based on results of a number of simulations. The cluster design selected for experimental work is shown in Figure 2. Simulations were performed using the commercial software package Nova Flow & Solid CV™ [6]. For reliable input from simulation, thermal properties for the shell material were measured in order to produce data for simulation software. Thermo-physical properties for the Udimet 500, the cast alloy were calculated with JMatPro™, [7], and are shown in table 1.  $f_l$  represent fraction liquid during solidification,  $\rho$  density of the metal,  $\kappa$  thermal conductivity,  $H$  enthalpy and  $\mu$  viscosity. Well established principles for gating design from previous work [2] [8] were considered to design a cluster. The ceramic shell material used for the experimental work was water based colloidal silica. The inner most layer consisted of  $CoAl_2O_4$  as a grain refiner and colloidal silica bound  $ZrSiO_4$  with Alumina oxide as stucco. Priming layers consisted of colloidal silica with a 325-200 mesh zircon flour. Alumina with a mesh size of 90-54 was used as stucco. For back up layers colloidal silica with a 200 mesh aluminium silicate slurry was used. 16-30 mesh aluminium silicate was used as stucco in backup layers. The shell properties were measured empirically. The specific heat capacity  $C_p$  of ceramic mould was measured with a differential scanning calorimeter Netzsch STA 404C™ equipment at a temperature range between 25°C to 1200°C as shown in Figure 3 (a).

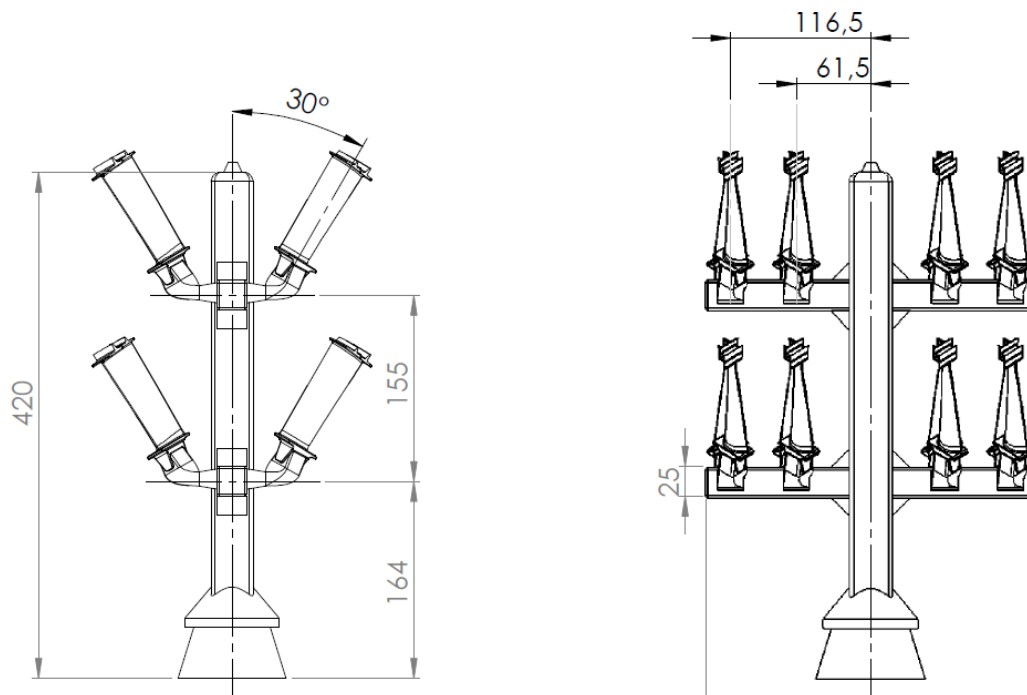


Fig. 2. Tree design for blade casting, all dimensions in millimetres

Table 1.

Thermo-physical properties for the Udimet 500™ used in simulation [7]

| $T$ (°C) | $f_l$ (-) | $\rho$ (kg/m <sup>3</sup> ) | $\kappa$ (W/m°C) | $H$ (J/kg°C) | $\mu$ (Pa s) |
|----------|-----------|-----------------------------|------------------|--------------|--------------|
| 1350     | 1         | 7230                        |                  | 8020         | 7.2          |
| 1325     | 0.40      | 7355                        |                  | 3275         | 7.7          |
| 1300     | 0.28      | 7425                        |                  | 2404         | 8.3          |
| 1275     | 0.10      | 7464                        |                  | 1317         | 9.1          |
| 1250     | 0.09      | 7490                        |                  | 996          | 10           |
| 1225     | 0.07      | 7508                        |                  | 1099         | 10.8         |
| 1200     | 0.05      | 7526                        | 30.5             | 781          | 11.7         |
| 1150     | 0         | 7526                        | 30.5             | 781          | 11.6         |
| 1100     |           | 7588                        | 28.8             | 627          | 12.9         |
| 1000     |           | 7767                        | 26.2             | 845          |              |
| 900      |           | 7726                        | 24.2             | 722          |              |
| 800      |           | 7777                        | 22.6             | 569          |              |
| 700      |           | 7821                        | 21.1             | 553          |              |
| 600      |           | 7863                        | 19.6             | 535          |              |
| 500      |           | 7903                        | 18.1             | 517          |              |
| 400      |           | 7941                        | 16.6             | 500          |              |
| 300      |           | 7977                        | 15               | 484          |              |
| 200      |           | 8010                        | 13.4             | 467          |              |
| 100      |           | 8042                        | 11.8             | 449          |              |
| 25       |           | 8064                        | 10.5             | 433          |              |

In order to measure thermal diffusivity  $\alpha$  of the mold, measurements were taken at temperature intervals 900 - 1300°C using a Laser-Flash Netzsch LFA 427/4/G™. The values of thermal diffusivity with respect to temperature are shown in Figure 3 (b). Density was measured in a temperature range between 25°C and 1200°C using a Netzsch DIL 402C/4/G™ dilatometer and the values of density vs. temperature are shown in Figure 3 (c). Thermal conductivity was calculated from thermal diffusivity, specific heat and density measurements using following expression [9].

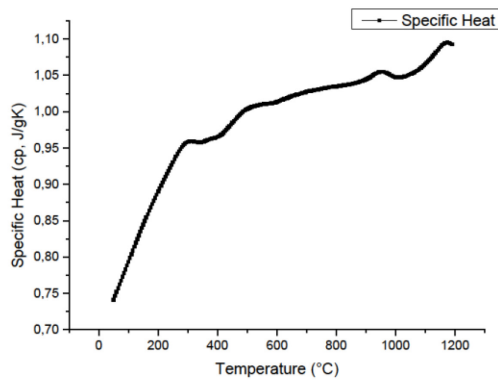
$$\lambda(T) = \alpha(T)\rho c_p(T) \quad (8)$$

Various patterns and thickness of insulation were applied to control heat flow and cooling rate in the airfoil. The intent was to control the solidification rate and direction. Table 2 describes the different types of insulations pattern and thickness used in the casting trials. The casting trials were performed according to experimental set up presented in Table 3. All castings were made in vacuum furnace. The time to cast (from preheat oven to pouring of tree) was kept constant for all the castings. The vacuum level ( $7 \cdot 10^{-4}$  mbar) in the furnace was kept constant and the castings conditions were kept as identical as possible.

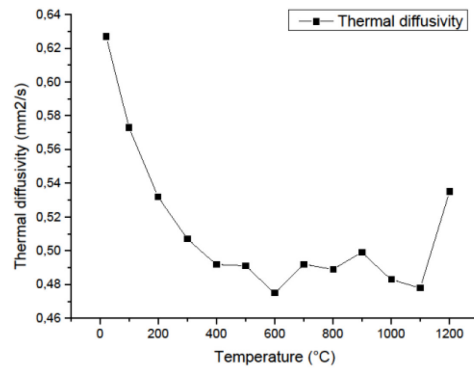
Table 2.

Insulation types and explanation

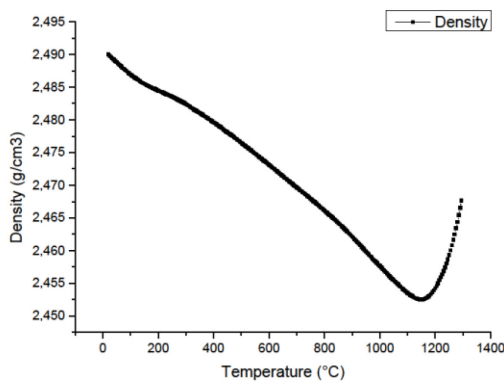
| Insulation type | Explanation   |
|-----------------|---|
| Type 1          | No insulation.  |
| Type 2          | 6 mm Complete air-foil.   |
| Type 3          | 12 mm Complete air-foil.  |
| Type 4          | 6 mm on bottom half at root side of air-foil and 12 mm on top half.                       |
| Type 5          | 6 mm on bottom half at root side of air-foil and 12 mm on top half + 6 mm at tip shroud.  |
| Type 6          | 12 mm on bottom half at root side of air-foil and 6 mm on top half.                       |
| Type 7          | 6 mm on 2/3 of bottom side at root of air-foil and 12 mm on 1/3 of top.                   |
| Type 8          | 6 mm on 1/3 of bottom side at root of air-foil , 12 mm on middle and 18 mm on 1/3 of top. |



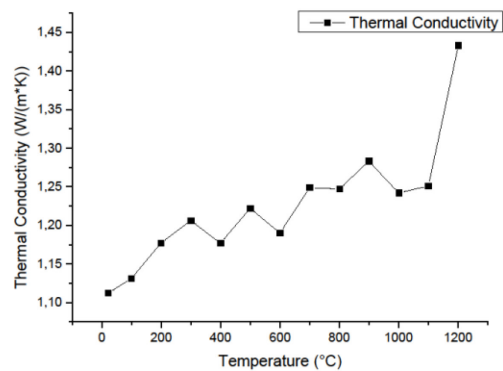
a) Specific heat of shell measured at different temperatures



b) Thermal diffusivity of shell measured at different temperatures



c) Density of shell measured at different temperatures



d) Thermal conductivity of shell measured at different temperatures

Fig. 3. Thermo-physical properties of the shell used in simulation

Table 3.

Design of experiments

| Insulation type | Temp. 1500°C      | Temp. 1520°C      | Temp. 1540°C      | Temp. 1560°C      |
|-----------------|-------------------|-------------------|-------------------|-------------------|
| Type 1          | 9 and 11 mm Shell |
| Type 2          | 9 and 11 mm Shell |
| Type 3          | 9 and 11 mm Shell |
| Type 4          | 9 and 11 mm Shell |
| Type 5          | 9 and 11 mm Shell |
| Type 6          | 9 and 11 mm Shell |
| Type 7          | 9 and 11 mm Shell |
| Type 8          | 9 and 11 mm Shell |

### 3. Results

To find effect of shell thickness and insulation on shrinkage porosity and grain at different casting temperature, results of experiments were statistically analysed using the commercially available statistical software, OriginPro™ [10]. For grain size evaluation, section closer to the root of the blade (the area which is more prone to the large grain size) was cut and evaluated using

optical microscopy. Figure 4 shows the location of cut sections for microscopy.

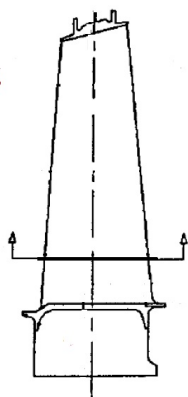
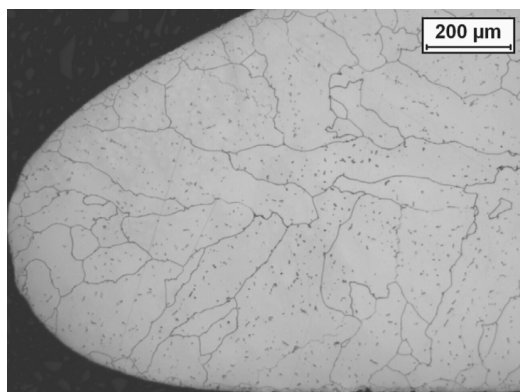


Fig. 4. Sample location for micro structure evaluation.

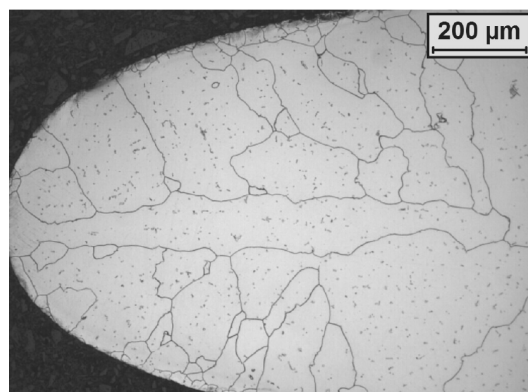
The area with large grains is measured by etching and manually measuring surface area of zone that is affected by coarse and columnar grains. The shrinkage porosity was manually measured from the X-ray films.

### 3.1. Effect of shell thickness on porosity and grain size

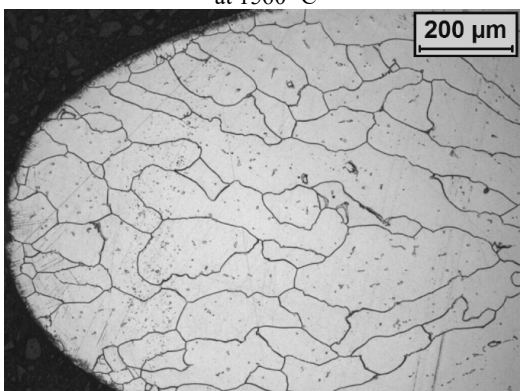
Shell thickness was observed to have very significant effect on shrinkage. It was possible to reduce size of shrinkage by increasing shell thickness. The effect of varying shell thickness on porosity and grain size at different temperature is presented in the graphs in Figure 7 (a) and (b). It was observed that increased shell thickness resulted in less shrinkage as shown in 7 (a).



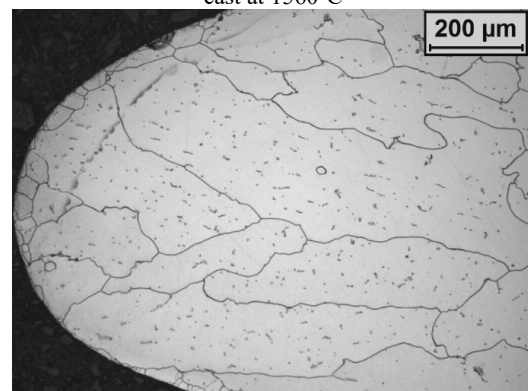
a) Grain size at leading edge of the blade cast with 9 mm shell cast at 1560 °C



b) Grain size at leading edge of the blade cast with 11 mm shell cast at 1560 °C



c) Grain structure in leading edge of blade at cast temperature 1520 °C with 11 mm shell



d) Grain structure in leading edge of blade at cast temperature 1560 °C with 11 mm shell

Fig. 5. Effect of temperature and shell thickness on grain size in a selected section shown in figure 4

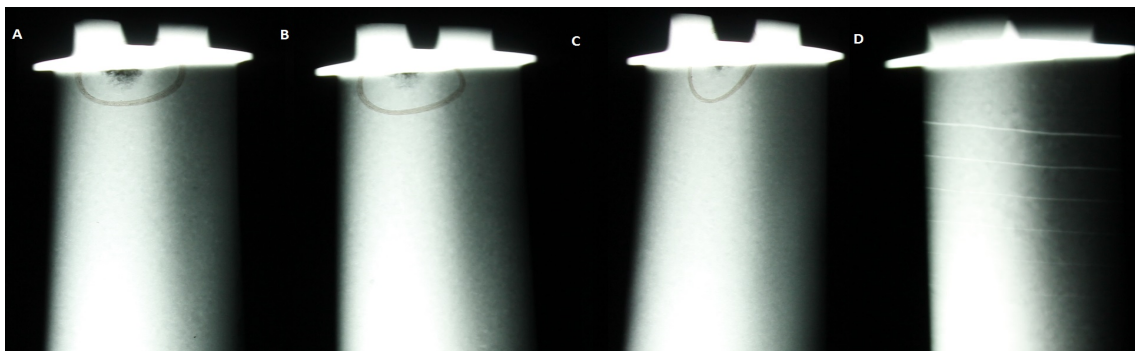


Fig. 6. Indication of porosity at different cast temperatures A) 1500 °C, B) 1520 °C, C) 1540 °C, D) 1560 °C

The graph shows the size of shrinkage at chord-tip shroud junction cast at four different casting temperature in ceramic shell made in two different thickness. Size of shrinkage at the chord-tip shroud junction dropped significantly by increasing shell thickness (by adding more layer of ceramic during shell building process), however effect of increased shell thickness on grain size was not significant as shown in 7 (b) and 4. Figure 5 (c) and (d) shows approximately same size of grains at both 9 mm and 11 mm shell thickness.

### 3.2. Effect of temperature on shrinkage and grain size

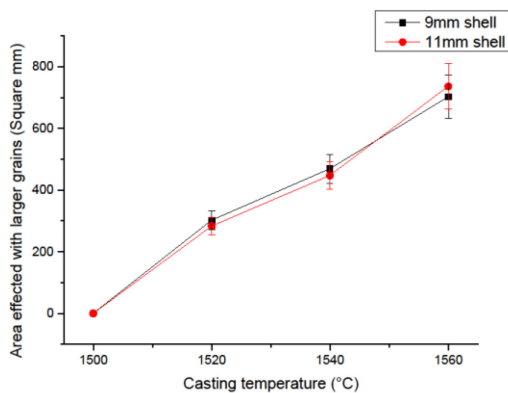
Geometries were cast at different temperatures to observe the effect of casting temperature on porosity and grain size. The best results in terms of shrinkage were observed at 1560 °C as shown in the X-ray film in Figure 6, however a coarse grain structure was observed at the root of blade as shown in Figure 5 (a) and 5 (b). Graph in figure 7 (a) shows that at lower casting temperature, i.e. 1500 °C, very large pores appeared at the chord-tip shroud junction. With an increase in casting temperature, size of shrinkage pore at chord-tip shroud junction dropped, however, an increase in grain size at the root of blade was observed as shown in figure 7 (b). Graph in figure 7 (b) shows the increase in area affected by larger grains at the root of blade as a result of increase in casting temperature. It was possible to obtain a fine-grain microstructure at lower casting temperatures, for example, 1520 °C and 1500 °C however large shrinkage at chord-tip shroud junction appeared at all these temperatures in uninsulated clusters with both 9 mm and 11 mm shell, however, at 11 mm size of shrinkage was significantly small as shown in 7 [a]. It can be seen

in X-ray images of these blades shown in Figure 6 that the extent of shrinkage increases with decreasing casting temperature.

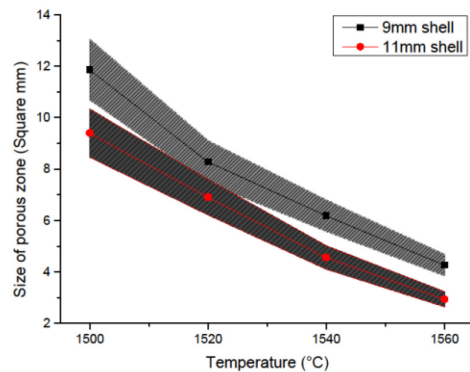
### 3.3. Effect of insulation on porosity and grain size

To investigate the effect of insulation on the shrinkage porosity inside the air-foil, only air-foils were insulated. Variation in insulations patterns and thickness significantly affected the size of the porosity as shown in Figure 7 (c). Types of insulations are explained in table 3. In uninsulated geometries, shrinkage at chord-tip shroud junction appeared at all casting temperatures, however, similar to pattern appeared in section 3.1, size of shrinkage dropped with an increase in casting temperature. It was observed that adding thicker insulation, for example, insulation type 3 can help to minimize the size of shrinkage pore, however, it resulted in large grains at the root of blade. Graph in 7 (d) shows the effect of insulation on the size of area affected by larger grains close to the root of blade. Insulation at blade geometry did not effect the size of grains at lower casting temperature, i.e. 1500 °C, however, with an increasing casting temperature, large grain appeared at the root of blade. The extent of area affected by large grains was dependent on the thickness and location of the insulation as explained in table 3.

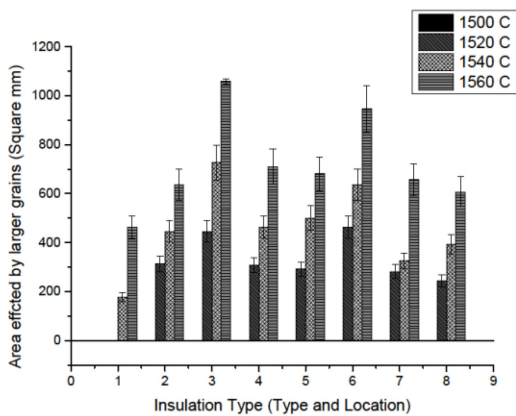
To further determine effect of insulation on fillability and grain size, trials were also performed using insulation at the feeder and in-gates. It was observed that if feeder and in-gates are insulated, larger grains can appear at the root of blade, i.e. adjacent to the feeder even at low temperature, for example, at 1500 °C. No significant effect of insulated in-gates and feeders was observed in terms of fillability.



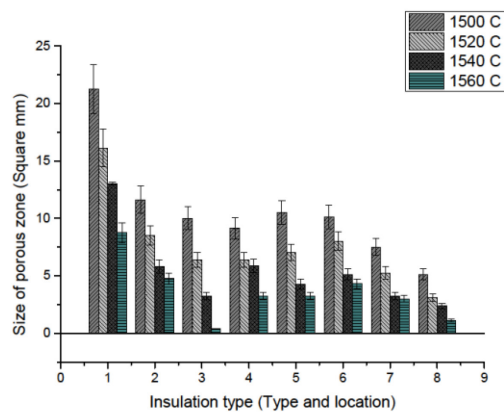
a) Effect of casting temperature on Porosity at two different shell thickness



b) Effect of casting temperature on grain size at two different shell thickness



c) Effect of insulation type on size of porosity at different temperatures



d) Effect of insulation type on grain size at different temperatures

Fig. 7. Effect of casting parameters on shrinkage porosity and grain size

## 4. Discussion

Casting temperature, insulation and shell thickness appeared to be key process parameters for eliminating shrinkage porosity, misruns and non-uniform grain structure as shown in graphs 7 (a), (b), (c) and (d). It was observed that eliminating shrinkage and misruns while maintaining a fine-grained micro structure required a trade-off. At higher temperature i.e. 1560 °C shrinkage porosity was completely avoidable due to the prolonged feeding of melt as shown in figure 6. However high casting temperature resulted in coarse grains at the root of the blade due to higher thickness at root and high heat mass from the adjacent feeding arm. Figure 5 (a) and (b) shows the large grains at the root of the blade cast at 1560 °C, regardless of shell thickness. At lower casting temperature, e.g. 1520 °C shrinkage porosity was avoidable by increasing the shell thickness without increasing the size of grains at the root of the blade as shown in 7 (a) and (b), where effect of casting temperature on grain size and porosity at two shell thickness is presented. Increased shell thickness as well as the application of insulation to the shell also serves to decrease

the cooling rate and thereby to limit dendrite arm length and thus the width of mush. The best results were obtained by minimizing cast temperature, adding insulation that allows faster cooling at the root of blade to limit grain size while slowing the cooling in thin sections which along with increased shell thickness control the width of mush. Figure 7 (c) and (d) describes the effect of different insulation patterns on grain size and shrinkage porosity.

In thin section, increasing shell thickness and thus increasing the capacity of the mould to absorb heat at initial phase of solidification lead to a steeper thermal gradient at the metal/mould interface [11]. A steeper thermal gradient hindered the growth of dendrite arms and improved the fillability in the thin sections and feed of metal to the shrinkage pores. However, no significant effect of increased shell thickness on the grain size was observed which can be attributed to the fact that effect of shell thickness on thermal gradient is for very short period of time, i.e. one or two initial seconds of solidification process after mould filling. These initial few seconds of solidification are very critical for dendrite growth [11] and thus for shrinkage porosity in thin sections of the blade, however not at the time scale where grain formation occurs, especially at the root of blade where cooling rate is slower

due to the adjacent feeder and thus extra heat mass. Grain size appeared to be dependent on available heat mass and cooling rate. At higher casting temperature, presence of extra heat mass above the root of the airfoil resulted in much slower cooling rate as compared to thin sections and thus larger grains in the root of the blade. The effect of casting temperature on grain size in a section shown in figure 4 is presented in graph 7 (b). In the presence of steep thermal gradient, an insulation pattern that allows slower cooling in the thin section while faster cooling in thicker section can help to avoid shrinkage porosity as well as uneven grain structure.

## 5. Conclusion

It has been observed that the thickness of the ceramic shell strongly influences shrinkage. The heat absorbing capacity of ceramic is determined by shell thickness, which is critical for casting of thin, complex shapes.

In thinner sections and at sharp junctions, the heat absorbing capacity is important due to its effect on the heat transfer coefficient and the thermal gradient in the metal adjacent to the mould wall. Increasing the heat absorbing capacity of ceramic shell helps to maintain a high thermal gradient between melt and mold for a longer time interval. The width of mushy zone decreases with increasing thermal gradient making possible feed of metal to shrinkage pores.

Adding insulation at thinner sections also slows the cooling rate which consequently minimizes the dendrite length resulting in a more planar solidification front. The conditions achieved through the higher thermal gradient and slower cooling rate keeps the width of mush shorter which allows metal feed through growing dendrite arms for a longer distance and thus helps to reduce shrinkage not only at points where solidification front meets but also between the growing dendrites.

## Acknowledgement

The authors would like to express their sincere gratitude to Jon A. Dantzig for helpful discussions. We also acknowledge Foundry

Research Institute in Krakow for conducting test on ceramic shell properties as part of joint study within CleanSky-LEAN project. Authors also thankfully acknowledge the financial support of the Innofactory program at Mälardalen Högskola funded through KK-Stiftelsen.

## References

- [1] Fredriksson, H., Åkerlind, U. (2006). *Materials processing during casting*. (1st ed.). West Sussex: John Wiley & Sons Ltd.
- [2] Beeley, P.R., Smart, R.F. (1995). *Investment Casting* (2nd ed.). London: The Institute of Materials.
- [3] Dantzig, J.A., Rappaz, M. (2009), *Solidification*. (1st ed.) Lausanne: FPFL Press.
- [4] Carlson, K.D. & Beckermann, C. (2009). Prediction of shrinkage pore volume fraction using dimensionless niyama criterion, *Metallurgical and Materials Transactions A*, vol. 40 (A), 163-175, DOI: 10.1007/s11661-008-9715-y.
- [5] Porter, D.A., Easterling K. E. (1981). *Phase Transformations in Metals and Alloys*. (1st ed.). Boca Raton: CRC Press.
- [6] Nova Flow & Solid CV, [Computer software]. (2013), Version 4.60r3.
- [7] JMatPro, [Computer software]. Sente Software Ltd, Retrieved from (www.sentes.com).
- [8] Li, D.Z., Campbell, J. & Li, Y.Y. (2004). Filling system for investment cast Ni-base turbine blades, *Journal of Material Processing Technology*, vol. 148, 310-316. DOI: 10.1016/j.jmatprotec.2004.02.032.
- [9] Konrad, C.H., Brunner, M., Kyrgyzbaev, K., Völkl, R. & Glatzel, U. (2011). Determination of heat transfer coefficient and ceramic mold material parameters for alloy IN738LC investment castings, *Journal of Materials Processing Technology*, vol. 211, 181-186. DOI: 10.1016/j.jmatprotec.2010.08.031.
- [10] Origin, [Computer software]. OriginLab, Northampton, MA.
- [11] Fredriksson, H. & Åkerlind, U. (2012). *Solidification and crystallization processing in metals and alloys*, (1st ed.). West Sussex: John Wiley & Sons Ltd.